IEEE Access
Multidisciplinary | Rapid Review | Open Access Journal

Received July 21, 2020, accepted July 23, 2020, date of publication July 29, 2020, date of current version August 10, 2020.

Digital Object Identifier 10.1109/ACCESS.2020.3012793

An Ultra-Wideband Rectangular Dielectric Resonator Antenna With MIMO Configuration

MOHAMMAD MUZAMMIL SANI, (Member, IEEE), RAKESH CHOWDHURY, (Member, IEEE), AND RAGHVENDRA KUMAR CHAUDHARY, (Senior Member, IEEE)

Department of Electronics Engineering, IIT (Indian School of Mines), Dhanbad 826004, India

Corresponding author: Mohammad Muzammil Sani (sani.mdmuzammil@gmail.com)

ABSTRACT A Coplanar waveguide (CPW) fed multi-permittivity and stair shaped dual rectangular dielectric resonator antenna (RDRA) has been designed for ultra-wideband (UWB) applications in multiple-input multiple-output (MIMO) configuration. Isolation improvement has been obtained by means of modified CPW feeding and a metallic diagonal stub in the proposed structure. The simulated results have been validated by prototype designing and performing measurements. The electrical size of the proposed antenna configuration is $1.12\lambda_0 \times 1.12\lambda_0 \times 0.25\lambda_0$. The measured input impedance bandwidth of the antenna is 153.6% (1.6-12.2 GHz) with a minimum of 25 dB isolation between the radiators in the operating band. Measured results illustrate the satisfactory performance of proposed UWB MIMO antenna with a low envelope correlation coefficient and low mutual coupling throughout the desired frequency range.

INDEX TERMS Ultra-wideband, dielectric resonator antenna, isolation.

I. INTRODUCTION

There are several benefits of ultra-wideband (UWB) technology like low cost, high data rate, etc. [1], [2]. The federal communication commission (FCC) has defined frequency range of 3.1-10.6 GHz for ultra-wideband unlicensed band which has drawn attention in wireless sensor networks, wireless healthcare systems. UWB antennas are facing some challenges in terms of electromagnetic interference, signal path fading etc. [3]–[8] and to resolve these issues, multiple-input multiple-output (MIMO) antenna systems are being designed with UWB technology. MIMO antennas are able to transmit multiple de-correlated signals with same power level simultaneously through spatially parallel channel [9], [10]. The MIMO system was used to limit the degradation caused by multipath propagation [11]–[14]. The diversity performance of MIMO antenna is required low envelope correlation coefficient values, and MIMO can be categories in the single radiator and multiple radiators [15]–[17]. Thus, designing of UWB antennas in MIMO arrangement is needed to enhance the antenna performance. Moreover, the metallic antenna becomes a poor radiator at higher frequencies and may be replaced by a dielectric resonator antenna (DRA). DRAs offers several advantages such as low losses, high radiation efficiency, less surface wave loss and large impedance bandwidth [18]–[21].

The associate editor coordinating the review of this manuscript and approving it for publication was Sudipta Chattopadhyay.

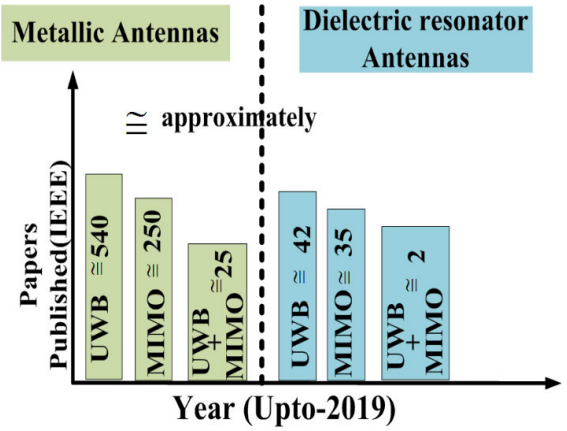

FIGURE 1. A pictorial description is showing flow chat of published papers from the literature survey.

Literature survey reveals that extensive research papers are available in UWB and MIMO patch antennas independently. Also, a considerable amount of study has been done on UWB using patch antennas for MIMO applications. In the context of a dielectric resonator as radiating element, research conducted on simultaneous operation of UWB and MIMO technology is very few in literature. A pictorial graph has been shown in Fig. 1, where the amount of research conducted in different concerned areas has been collected through a literature survey. Thus, from observation, it has

TABLE 1. Comparison of Wideband MIMO DRA antenna with proposed work.

Ref. (Year)	Operating frequency band	Edge to edge separation (mm)	Gain (dB)	Total Size (λ_o x λ_o x λ_o)mm^3	Features		Isolation (dB)	B.W%
					UBW	MIMO		
[22],2019	3.55-16.0 GHz	No	9.9	1.08×0.89×0.36	✓	×	No	133
[23], 2019	3.2-11.35 GHz	No	3.3	0.04×0.43×0.82	✓	×	No	112
[24], 2019	3.5-4.95 GHz	40	6.2	0.48×0.48×0.36	×	✓	28	38.5
[25], 2017	4.89-9.61 GHz	13	7.9	1.43×1.43×0.42	×	✓	20	65
[26], 2014	2.4-12.0 GHz	35.2	5	3.60×3.60×0.55	✓	✓	10	133.3
[27], 2017	3.29-10.74 GHz	11	5.3	0.68×0.68×0.12	✓	✓	17	106
Proposed	1.6-12.2 GHz	12.44	4.72	1.12×1.12×0.25	✓	✓	25	153.6

been found that very few research study has been conducted on these three technologies (DRA + UWB + MIMO) altogether, which can make antenna performance more efficient. This is the research gap identified, which led to the urge for designing UWB antennas using dielectric resonators in MIMO arrangement. Although, there are some antenna designs proposed in recent years which are listed in Table 1 and compared with proposed work. In [3]–[8], ultra-wideband DRA has been proposed but the features of MIMO systems are missing. Again, some MIMO designs were also proposed [24], [25], but the feature of ultra-wide bandwidth is missing. In [26]–[32], authors have proposed a new compact DRA based ultra-wideband antenna designed in MIMO configuration. Motivated from [26], [27], a new ultra-wideband DRA is presented for MIMO applications in this article, and corresponding results are verified by measurements.

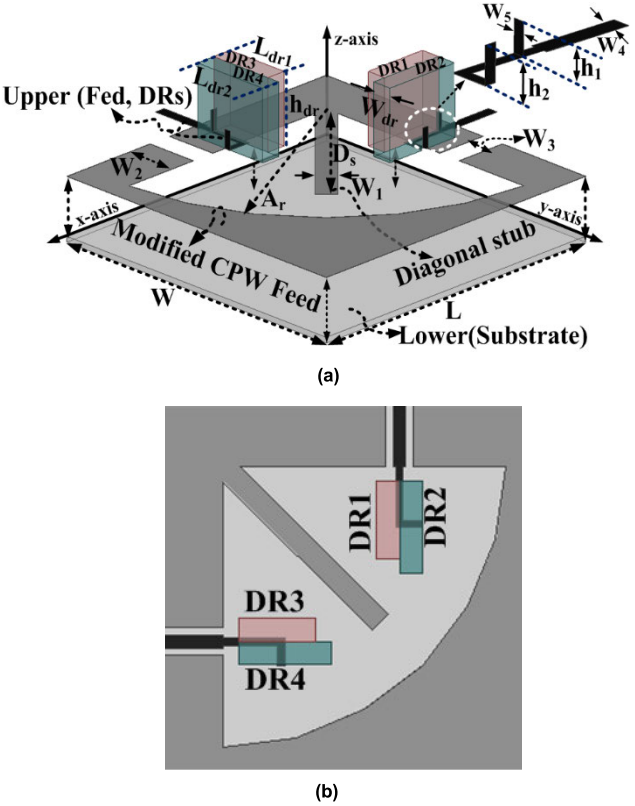

FIGURE 2. Schematic of proposed antenna (a) 3-D view and (b) top view [all dimension are in mm: W =48, W1=3, W2=8, W3=3.6, W4=1.6, W5=1, Wdr =3, hdr =10, hsubstrate =0.8, L =48, Ds =30, Ldr1=10, Ldr2=12, h1=3 and h2=2.6ε_{dr}2 and ε_{dr}4 = ε_r = 9.8 and ε_{dr}1 and ε_{dr}3 ε_r = 20].

II. ANTENNA DESIGN EVOLUTION AND THEORY

A. ANTENNA CONFIGURATION AND FLOW DIAGRAM

The 3D-layout of the proposed UWB MIMO antenna based on modified co-planar waveguide feeding is shown in Fig. 2 with relevant dimensions provided in the caption. Fig. 3(a-b) shows the prototype of the proposed design. It consists of two pair of dual stair shaped RDRA of different permittivity ($\varepsilon_r = \varepsilon_r$ =9.8 and $\varepsilon_r = \varepsilon_r = 20$) which are placed at an orthogonal position. Next, a diagonal stub is overextended symmetrically in between DR assembly at an angle of 45° for manipulating the current path in order to improve coupling among the fields of both DRs. The modified arc shape (A_r) CPW feeding and diagonal stub (D_sD$_s$) is responsible for improving the isolation between the dielectric radiators.

Fig. 4 shows the chronology of the proposed antenna. The flow diagram expresses the design evolution of whole steps performed for achieving the ultra-wideband performance with good isolation. Initially, homogeneous rectangular DRAs is designed in orthogonal arrangement fed by an *L*–shaped microstrip feeding placed beneath the DRA with wide bandwidth performance obtained due to the co-planar waveguide feeding. In the second design step-2, the RDRA has been modified into stair–shaped form with multi-permittivity approach to achieve the ultra-wideband performance. In the remaining steps, the co-planar waveguide feeding has been modified into arc-shaped ground plane and a diagonal metallic stub has been introduced between the radiators. This is done in order to achieve the isolation between the DRA elements. Finally, incorporating these design paramters for getting isolation improvement in ultra-wideband antenna to get ultra-wideband MIMO antenna. Initially, an ultra-wideband DRA design is planned by optimizing the shape and permittivity of RDRAs.

Then, to achieve good isolation, CPW feeding is modified in arc-shaped, and a diagonal stub is added, which is further optimized to get the desired objective. There are few ultra-wideband antennas in MIMO configurations which uses

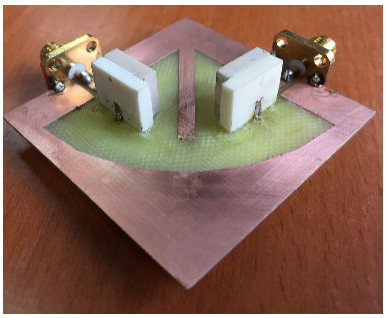

(a)

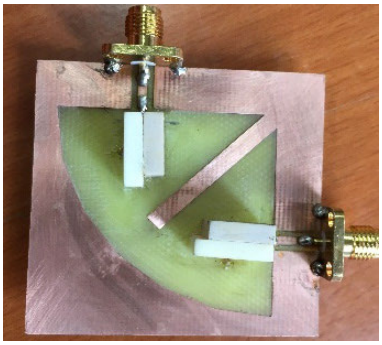

(b)

FIGURE 3. Prototype structure of the proposed antenna (a) 3-D view and (b) top view.

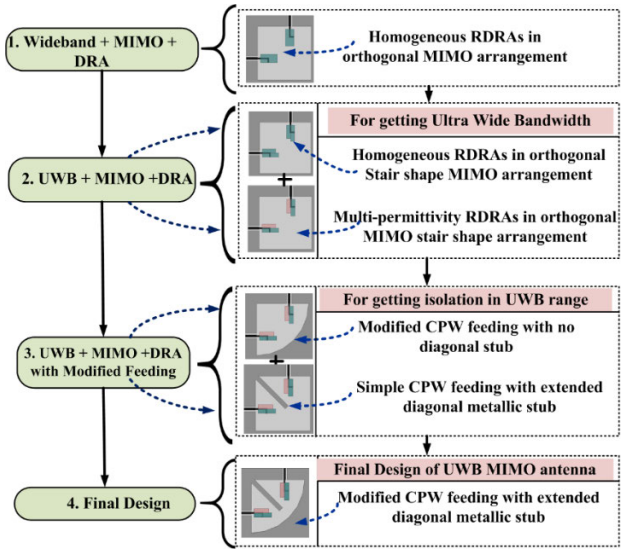

FIGURE 4. Flowchart showing the design procedure to achieve final proposed antenna configuration.

dielectric resonators as radiating element. This is because, getting a very good isolation between the radiators in an ultra-wide frequency range is difficult and also it is difficult to maintain that isolation in the entire band. This has been achieved in this paper by simultaneous effect of diagonal stub and co-planar waveguide feeding.

B. ANALYSIS OF ULTRA-WIDEBAND DESIGN

In this section, the process of achieving ultra-wide bandwidth is discussed, followed by the investigation of isolation improvement in next section. Simultaneous use of multi-permittivity dielectric resonators and stair shaped arrangement has been used for getting ultra-wideband response. The stair-shaped RDRA arrangement and the L-shaped feeding helps in exciting the fundamental TE_{111} and higher oreder TE_{113} mode and merging of them. Also, by using multi-permittivity approach the effective dielectric constant is reduced which leads to further reducing the radiation Q-factor and accordingly the impedance bandwidth increases. In Fig. 5(a) and Fig. 5(b) shows the S_{11} and S_{21} parameters for different antenna stages, respectively.

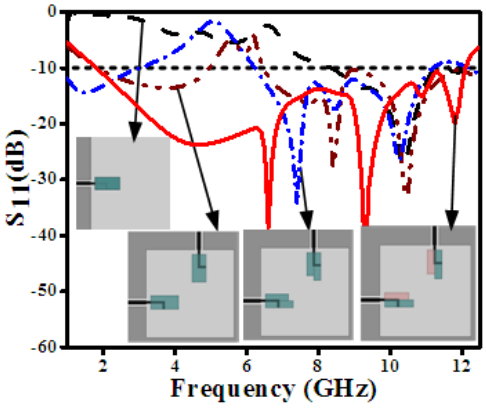

(a)

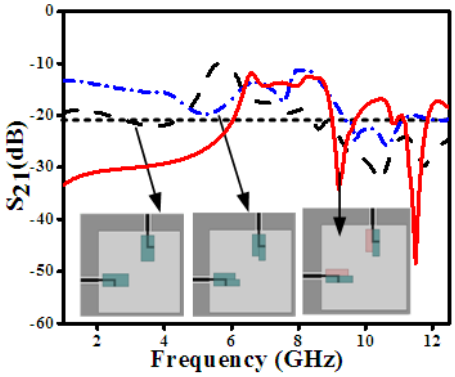

(b)

FIGURE 5. Simulated results of $|S_{11}|$ and $|S_{21}|$ for achieving ultra-wideband performance.

Initially, a single RDRA is excited by a microstrip network using CPW fed technique due to which one wideband is obtained at a higher frequency range. Another RDRA with same permittivity and same feeding is positioned in an orthogonal fashion. It has been observed that impedance bandwidth is increased in the form of triple band; however, isolation of approximately 11 dB is reported. Further, in the next step, shape of RDRAs is modified into stair shape form by removing a small portion along DRA length side. In this case, two bands are obtained but isolation is same. In the last step, different permittivity is used to increase the impedance bandwidth by merging of two band of the previous steps of antenna design. Here, the increasing of impedance bandwidth follows the multi-layer multi-permittivity (MLMP) concept, where DR1 and DR3 have $\varepsilon_r = 20$ whereas DR2 and

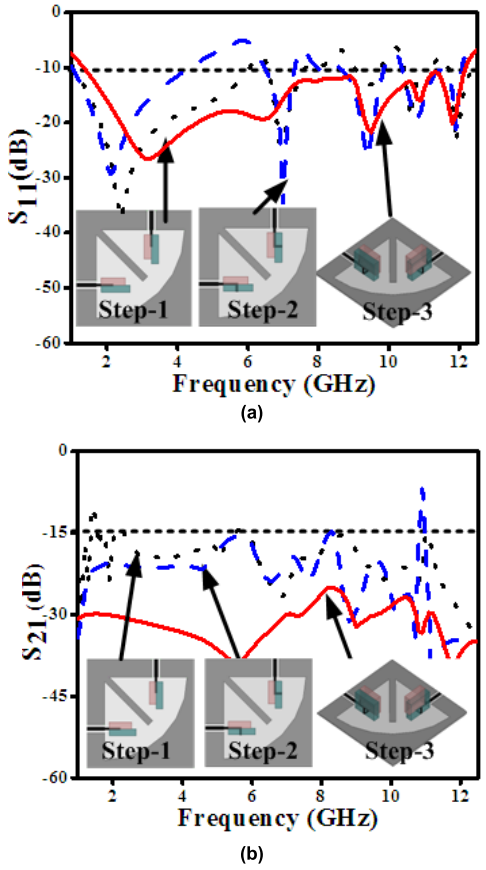

FIGURE 6. Simulation results for different feed steps of (a) $|S_{11}|$ and (b) $|S_{21}|$.

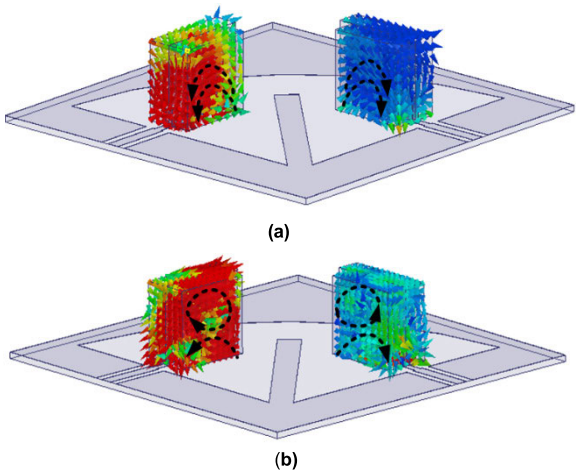

FIGURE 7. E-field distribution inside RDRAs at (a) TE_{111} at 4.8 GHz and (b) TE_{113} at 6.8 GHz.

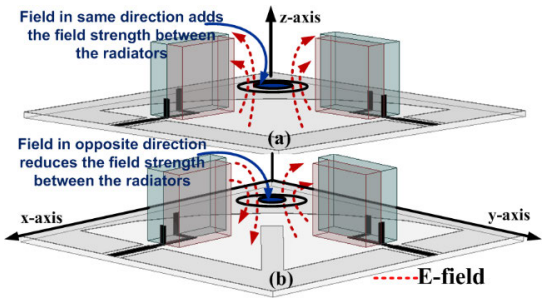

FIGURE 8. Schematic diagram of field orientation inside RDRAs.

DR4 have $\varepsilon_r = 9.8$ respectively. Fig. 6(a) represent the $|S_{11}|$ parameter for different feed steps used in different permittivity of RDRA. Initially, RDRAs is excited by a straight horizontal microstrip feed network as a result of which wideband is obtained at a lower frequency range. Next, the L-shape feed network is used for excitation of RDRAs. It has been observed that impedance bandwidth has decreased, but isolation between the radiators is almost the same throughout the operating frequency range in both steps of feed networks. The responsible modes excited in the DRA due to feed network and stair shape arrangement is responsible for wide bandwidth as dipslayed in Fig. 7.

Further, the proposed feed network is used for excitation of RDRAs. In Fig. 6(b), the isolation of antenna has been discussed by different steps of antenna design. In step-1 and in step-2, the isolation between the radiators is almost similar to week isolation. In the proposed antenna step (step-3), the antenna produced good isolation between the radiators, due presence of two isolation elements; one is a diagonal stub (D_s) and other is arc shape (A_r).

C. ISOLATION MECHANISM

The isolation reduction between the radiators with corresponding physics is explained through a schematic diagram as illustrated in Fig. 8. In physics, coupling or energy transfer at any region of space due to several sources of radiation is dependent on the interaction of field components at a particular region of space. Electric and magnetic fields are vector fields; thus, the amount of coupling depends on both net magnitude and direction of fields at a particular point. In this work, the idea is to excite the same modes ($\delta TE^{x}_{11} TE^{x}_{111}$ *and* TE^{y}_{111} δTE^{y}_{11}) in RDRAs in different phase so that the net direction of field components radiated from the RDRAs propagates in opposite direction and thus less energy is coupled between them. An extended diagonal stub is inserted between them and CPW feeding is modified to acquire the opposite field. Fig. 9 shows the radiated fields in same direction in the absence of diagonal stub and modified arc in the ground plane. Both RDRAs are influenced by the fields, thereby providing less isolation. But after the introduction of diagonal stub and modified arc ground plane, the net radiated fields propagate in the opposite direction, therefore, isolation between the radiators has enhanced. The E-field distribution in Fig. 9(a) are in the same direction and for Fig. 9(b), 9(c) and 9(d), it is in opposite direction.

The mutual coupling in the proposed design is improved by "two" alterations in the conventional CPW feeding. The first modification is done by changing the CPW feeding in arc shaped defined by the parameter Ar and secondly, an extended diagonal stub is inserted between the radiators defined by the parameter D_s.

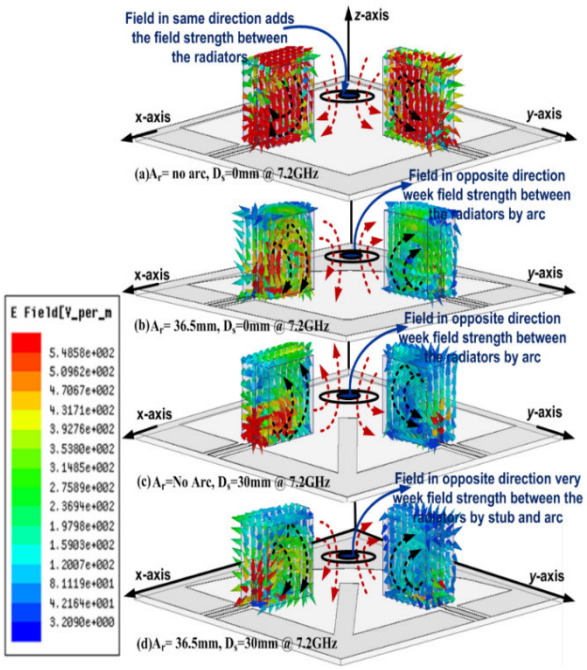

FIGURE 9. E-Field distribution inside the RDRAs at 7.2 GHz (a) without stub (D_S) and no arc (A_r), (b) without stub (D_S) and modified arc (A_r), (c) with stub (D_S) and no arc (A_r) and (d) with stub (D_S) and modified arc (A_r).

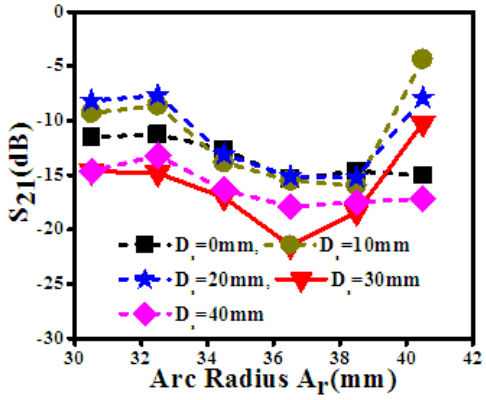

FIGURE 10. Simulated $|S_{21}|$ values with varying A_r at different values of D_S.

As the two pairs of rectangular dielectric resonator are excited by a CPW feeding, the return current (from the return conductor) is shared by both radiators, such that the common current induced in the ground plane significantly affects the electromagnetic interaction between them. Therefore, by variation in the return conductor design, a change in mutual coupling or isolation improvement is expected. For this purpose, the return conductor is slightly modified into arc-shaped at the outer edge of ground plane and its arc-radius is varied for different values of diagonal stub as plotted in Fig. 10. The second parameter is the diagonal stub whose length is varied in between the radiators. By changing D_s, the current at the two input terminals has been revised to excite the required modes in the DRA which results in reversing their phase. With the insertion of diagonal stub, the path

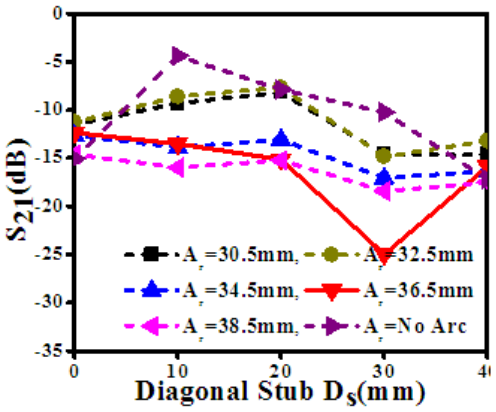

FIGURE 11. Simulated $|S_{21}|$ values with varying D_S at different values of A_r.

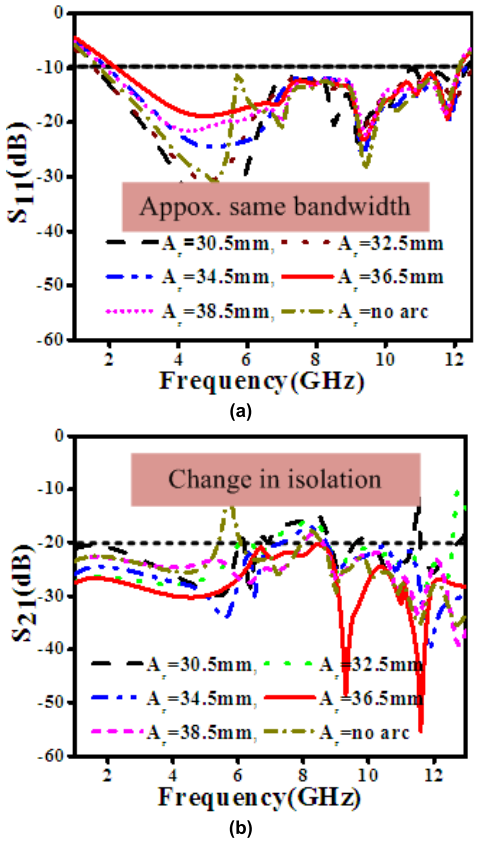

FIGURE 12. Simulated results of $|S_{11}|$ and $|S_{21}|$ by varying Arc radius (A_r).

length is altered in the return conductor such that current in the feeding strip responsible for exciting the dielectric resonator is also changed. Fig. 11 shows the maximum isolation achieved in the design by varying the diagonal stub length at different values of arc-radius. Thus, these two parameters A_r and D_s are responsible for changing the isolation level in the design. With reference to Fig. 10, it has been observed that maximum isolation is obtained at $D_s = 30$ mm with $A_r = 36.5$ mm. Next, With reference to Fig. 11, best isolation is obtained at an optimized value of $A_r = 36.5$mm. with $D_s = 30$ mm. Now, Fig. 12 shows

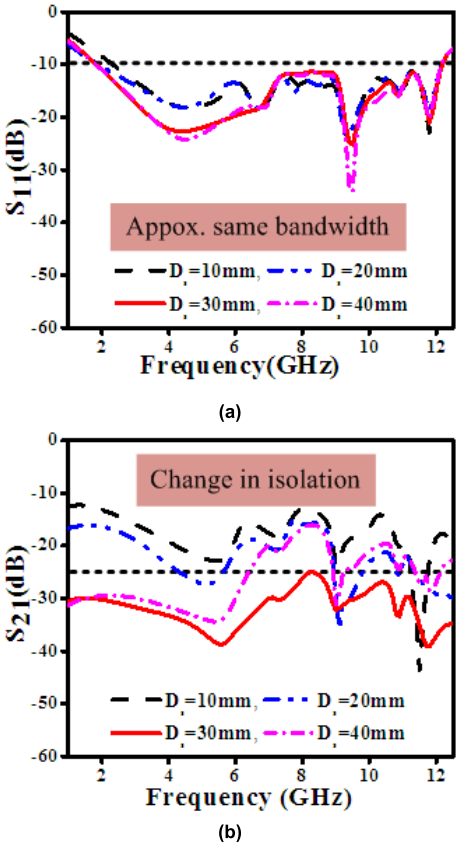

FIGURE 13. Simulated results of $|S_{11}|$ and $|S_{21}|$ by varying D_s strip.

the s-parameters of the proposed design for optimized D_s = 30 mm at different values of A_r. It has been observed that, the impedance bandwidth does not significantly change but a change is isolation is obtained. This is because, the impedance bandwidth is achieved due to the stair-shaped arrangement of DRAs and their multi-permittivity materials. Same result is obtained when s-parameters are plotted at optimized value of $A_r = 36.5$ mm at different values of D_s as shown in Fig. 13. In this case also, the impedance bandwidth nearly remains same but a change in the isolation significant. This analysis also confirms that the isolation in the proposed design is obtained due to the variation in the CPW feeding geometry while maintain ultra-wide bandwidth.

In short, In Fig. 12(a) and Fig. 12(b), the $|S_{11}|S_{11}$ and $|S_{21}|$ of the antenna design are shown. It is observed that no change in $|S_{11}|$ is noticed by varying the modified arc shape (A_r) radius values but $|S_{21}|$ has been changed. Similar analysis has been done by varying the stub length (D_s) and it has been observed that $|S_{11}|$ is almost same but $|S_{21}|$ is changed, which is shown in Fig. 13(a) and Fig. 13(a) respectively. The surface current distribution at 5.6 GHz is shown in Fig. 14 by varying stub length (D_s) from 0 mm to 30 mm. From this analysis, it is found that without diagonal stub, the surface current strength is almost the same in both port 1 and port-2 feed network port 2 feed network when the source is applied at port 1. When the diagonal stub is used and increased its length stub,

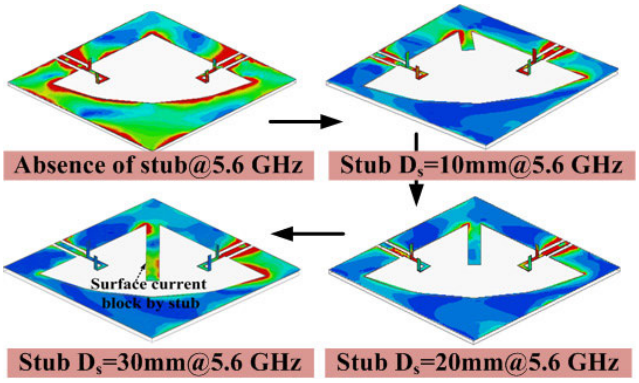

FIGURE 14. Surfaces current distribution by varying stub length D_s at 5.6 GHz.

the surface current is decreased from port 1 to port 2 due to manipulation of surface current distribution direction by the diagonal stub. The parametric analysis has been carried out for getting optimized value of antenna parameters. This optimized value is used to designed the proposed antenna and fabrication.

III. PARAMETRIC ANALYSIS

A. OPTIMIZATION OF DIELECTRIC CONSTANT (ε_r)

The concept of multi permittivity concept is used in this design in order to enhance the impedance bandwidth of proposed design [18]. As the Q-factor theory illustrates that resonance frequency is inversely proportional to the permittivity and radiation Q-factor is directly proportional to the permittivity of the DRA. Multi permittivity layers can have different radiation Q-factors and resonance frequencies. The multi permittivity arrangement could be used to control both radiation Q-factor and resonance frequency simultaneously. Here, optimizing the dielectrics constant values of the rectangular dielectric resonator (RDRs), optimum performance has been achieved. From Fig. 15(a) and Fig. 15(b) shows the S-parameters for different combination of dielectric constant of RDRAs (i.e DR1 and DR3 both are same permittivity, DR2 and DR4 both are same permittivity). However, from parametric analysis, it is observed that the combination of RDRAs with different permittivity constant (ε_{dr}(DR2 and DR4) = 9.8 and ε_{dr}(DR1 and DR3) = 20.0) has obtained best ultra-bandwidth and good isolation between the radiators. The impedance bandwidth is 153% and isolation is approx. 25 dB between the radiators at chosen value of permittivity.

B. OPTIIMIZATION OF LENGTH OF RDRs (L_{dr})

Stair shape RDRAs are mentioned in Fig. 16 to illustrate the parametric analysis for rectangular dielectric resonator (RDRs) length. The stair shape is obtained by optimizing the length of RDRAs. Here, the combination of DR1 and DR3 have same length whereas the combination of DR2 and DR4 have same length. In this case, stair shape arrangement is one of the approach for exciting multiple modes and merging them for wideband appicaitons due to which the bandwidth of the antenna is increased. In Fig. 16(a) and

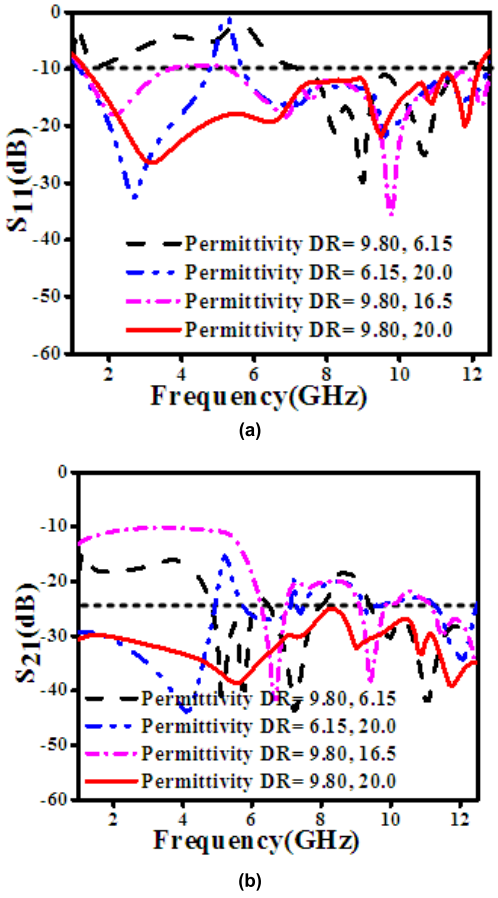

FIGURE 15. Simulated results of parametric analysis of dielectric resonator permittivity (a) $|S_{11}|$ and (b) $|S_{21}|$.

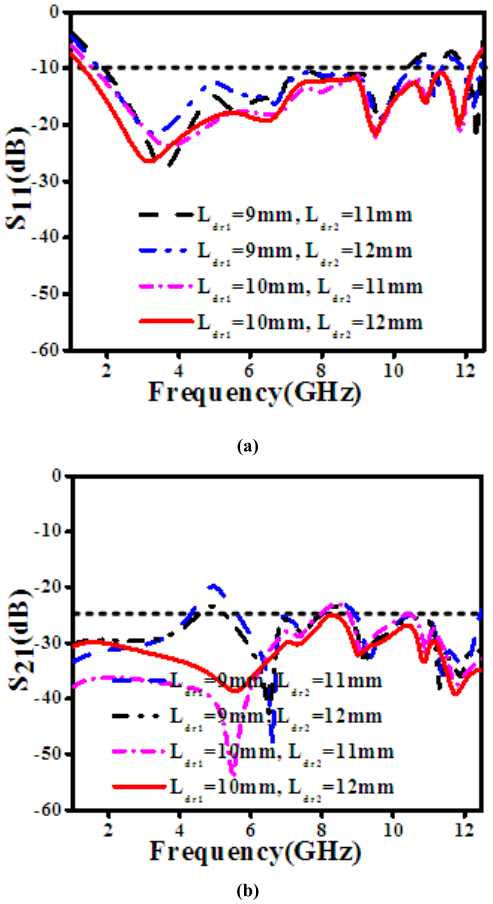

FIGURE 16. Simulated results of parametric of RDRAs lenght L_{dr1} and L_{dr2} (a) $|S_{11}|$ and (b) $|S_{21}|$.

Fig. 16(b), parametric analysis of DR1 length (L_{dr1}) and DR2 length (L_{dr2}) is represented. Here, it is clearly seen that different combination of L_{dr1} and L_{dr2} provides good impedance bandwidth and isolation between the radiators. By the analysis of this RDRs arrangements, it is noticed that the maximum impedance bandwidth and good isolation between the radiators at $L_{dr1} = 10$ mm and $L_{dr2} = 12$ mm has been found, which is shown in Fig. 16(a) and Fig. 16(b) respectively.

C. PARAMETRIC OF TOTAL ACTIVE REFLECTION COEFFICIENT (TARC)

For multi-port system scattering parameter is not enough to suitably characterize the MIMO antenna system. Total active reflection coefficient (TARC) is important parameter for multiport MIMO system antenna. The effects is took place into the consideration, when ports of MIMO antenna system are fed with different phases of signal. The TARC can be calculated by using this formula given by Eqn.1.

$$\Gamma_a^t = \sqrt{\left(\left|S_{11} + S_{12}\, e^{j\theta}\right|^2 + \left|S_{21} + S_{22}\, e^{j\theta}\right|^2\right)\Big/2} \qquad (1)$$

where θ is the phase difference between two feeding ports. As shown in Fig. 17, the TARC of the proposed antenna

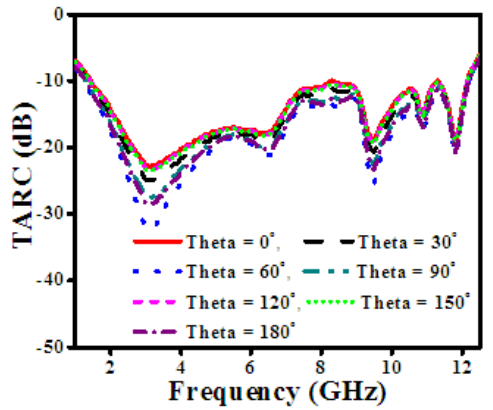

FIGURE 17. Simulated parametric analysis of TARC.

is illustrated. In Fig. 17 illustrated, the simulated TARC with phase varying from $\theta = 0°$ to 180° by the interval of 30°. It has been notice that the TARC throughout operating frequency band is similar the original behavior of the antenna characteristics.

D. PARAMETRIC OF VERTICAL STRIP POSITION (VSP)

In this section, illustration of vertical strip position (VSP) for antenna designing is performed. In VSP-1, one vertical strip is attached with both (DR1 and DR2) and other vertical

strip is attached with DR2 only. At this position, distance between the two vertical strips is maximum. Next in VSP-2, one strip is attached with both DRs (DR1 and DR2) and other strip attached with DR2, such that both strips are closed to each other. Again in VSP-3, one vertical strip is attached with DR1 and other vertical strip is attached at the middle of the DR2. Further in VSP-4, one vertical strip is connected with DR2 and other vertical strip is connected at the middle of the DR2. Finally in the proposed (VSP-5), one vertical strip is connected with both (DR1 and DR2) and one vertical strip connected at the middle of the DR2. From the microstrip transmission line theory, transmission line under the beneath of the dielectric resonator, strong coupling '*x*' is slightly shorter than one-quarter electrical wavelength of the resonance frequency.

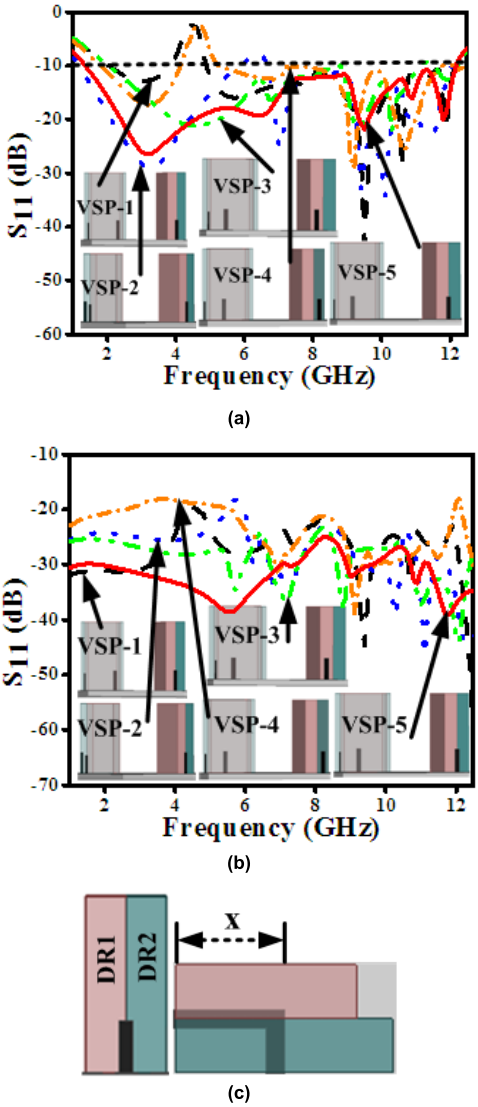

FIGURE 18. Simulated results of different vertical strip position (VSP) (a) $|S_{11}|$, (b) $|S_{21}|$ and (c) strip length (x).

As shown in Fig. 18, here 'x' is 7mm which is slightly shorter than the electrical wavelength at the resonance frequency, as shown in Fig. 18(c). From Fig. 18(a) and Fig. 18(b), the value of 'x' satisfies the position of vertical microstrip in case VSP-5.

E. GROUND PLANE ANALYSIS

To illustrate the effect of ground plane, the overall ground plane size has been increased to 60 × 60 mm^2 and 70 × 70 mm^2 while maintaining the location of rectangular DRAs same as of the proposed design (with 48 × 48 mm^2). Due to this, the arc radius value has changed. Now, we have already shown that the arc radius is responsible for altering the isolation performance while insignificant change in impedance bandwidth which is again verified here by plotting the s-parameters with different ground size. In order to address the situation when large ground plane will be required, we have performed some simulations considering large ground plane and the corresponding s-parameters are shown in Fig. 19. Thus, varying the ground plane size will significantly affect the isolation performance

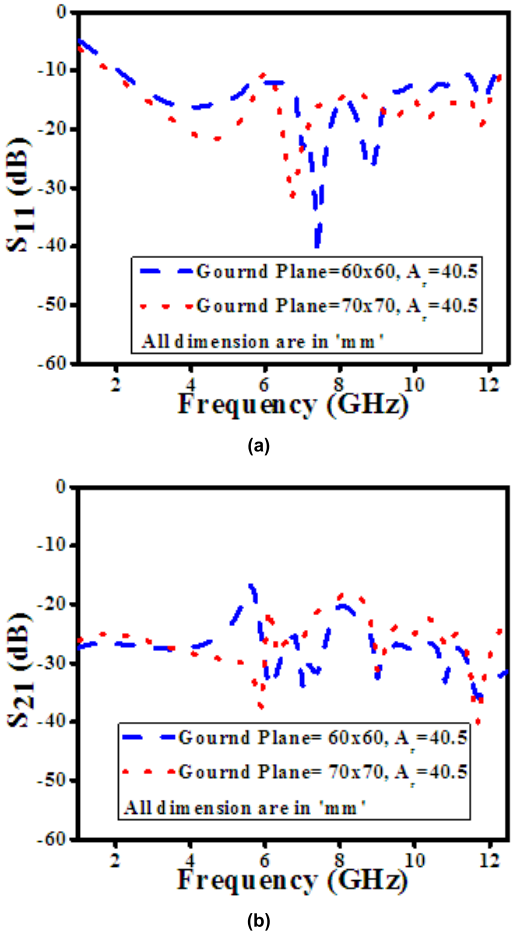

FIGURE 19. Simulation results for varying ground plane size (a) $|S_{11}|$ and (b) $|S_{21}|$.

IV. MEASURED RESULTS AND DISCUSSION

The proposed antenna design has been fabricated and simulation results have been verified. The input reflection

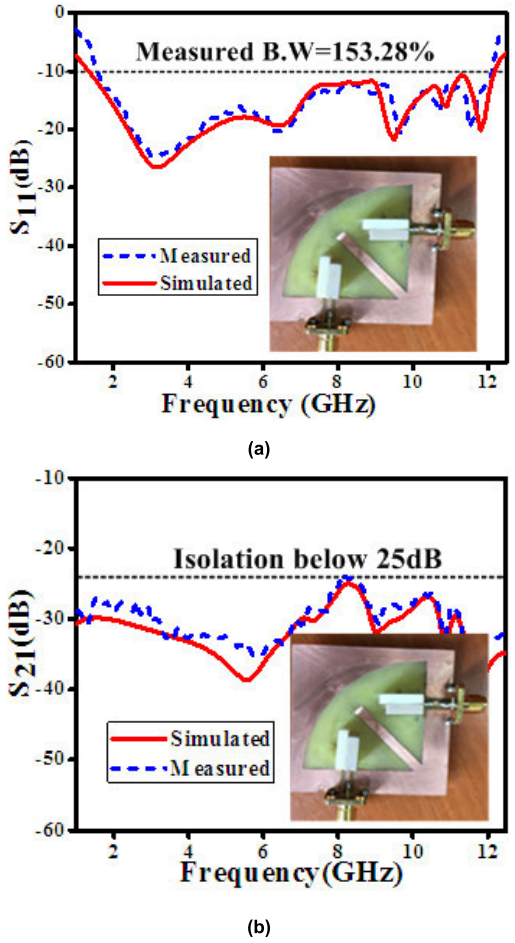

FIGURE 20. The simulated and measured S-parameters of the proposed antenna (a) $|S_{11}|$ and (b) $|S_{21}|$.

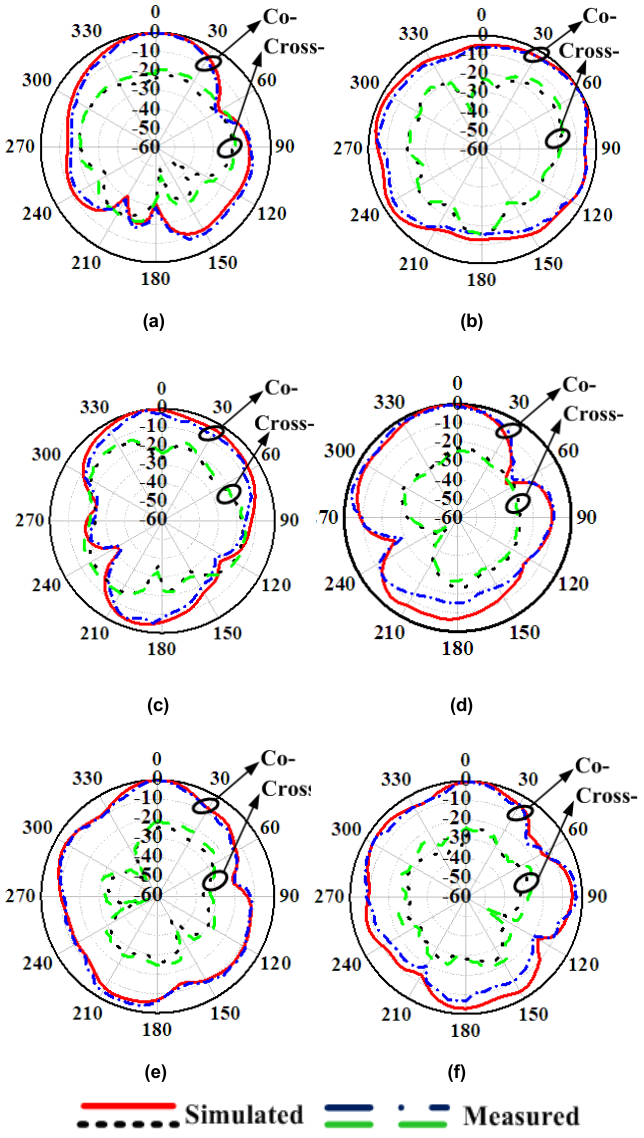

FIGURE 21. Simulated and measured normalized radiation pattern in *xz*-plane at (a) 3.1 GHz, (b) 5 GHz, (c) 7 GHz (d) 9.4 GHz and (e) 10.8 GHz and (f) 11.8 GHz.

coefficient measurement of the proposed antenna was performed by using the PNA network analyzer. The simulated and measured *S*-parameters results demonstrated a reasonable agreement, as shown in Fig. 20(a-b). From the measured result, it is clearly observed that the sufficient frequency band of 1.6 to 12.2 GHz for UWB MIMO DRA with 153.6% impedance bandwidth has been obtained which is shown in Fig. 20(a). While high isolation below 25 dB is achieved in the proposed design as shown in Fig. 20(b), due to the inclusion of the modified arc shape ground plane (A_r) and diagonal stub (D_s). In Fig. 21, the simulated and measured *xz*-plane radiation pattern at different frequencies 3.1, 5, 7, 9.4, 10.8 and 11.8 GHz. It has been perceived that good agreement between simulated and measured results in the broadside direction has been obtained. From radiation pattern plot at Fig. 21 in the we would like to say that, for a UWB antenna, the radiation pattern must be consistent throughout the operating band which is the objective to show the radiation pattern at different frequencies. Also, the co-cross difference is also more than 15 dB which is a standard acceptable value used in antenna technology. For the satisfactory performance of MIMO antenna has been required to evaluate the diversity performance of the proposed antenna by various parameters i.e. diversity gain (DG), envelop correlation coefficient (ECC) and channel capacity loss (CCL). Calculation of ECC by using S-parameters is defined as [33].

$$\mathrm{ECC} = \frac{\left|S_{11}^{*}S_{12} + S_{21}^{*}S_{22}\right|^{2}}{\left(1 - |S_{11}|^{2} - |S_{21}|^{2}\right)\left(1 - |S_{22}|^{2} - |S_{12}|^{2}\right)} \quad (2)$$

The directive gain can be calculated according to the following equation.

$$\text{Diversity Gain} = 10\sqrt{1 - \mathrm{ECC}^{2}} \quad (3)$$

The simulated and measured results of the proposed UWB MIMO antenna are in reasonable agreement. In Fig. 22, it is has been observed that across the entire operating band

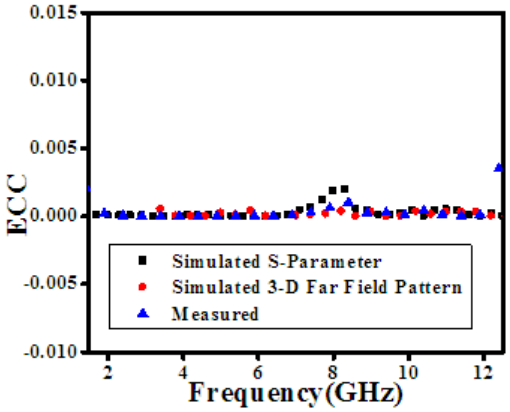

FIGURE 22. Simulated results of ECC of the proposed antenna.

the ECC <.003, which satisfies the low ECC criteria (ECC <0.3). Here, calculated results of ECC from *S*-parameter and 3-D far field pattern both are obtained almost similar throughout the operating frequency range. In Fig. 23(a), the diversity gain (DG) of antenna approximately 10 dB, which also fulfils the criteria.

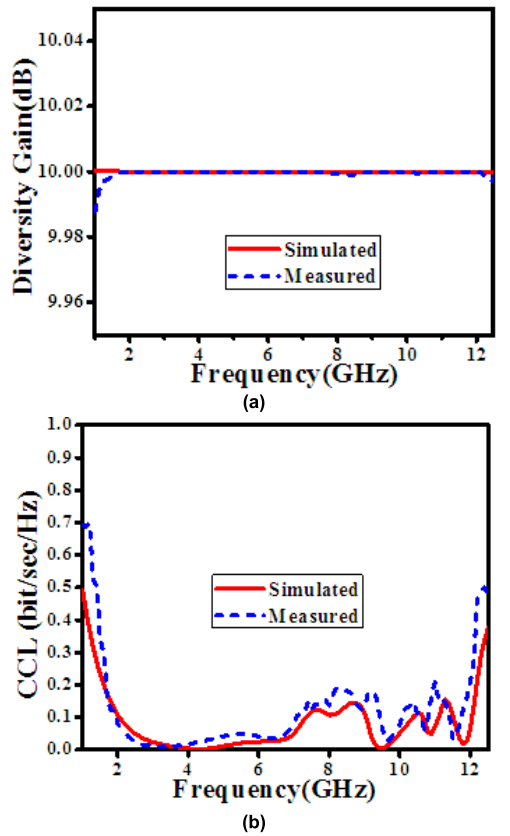

FIGURE 23. Simulated results of DG and CCL of the proposed antenna.

The channel capacity can be evaluated by the following formulas.

$$C_{loss} = -\log_2\left(det\left(\psi^R\right)\right) \tag{4}$$

The receiving antenna correlation matrix is represented by ψ^R and define as

$$\psi^R = \begin{pmatrix} \rho_{11} & \rho_{12} \\ \rho_{21} & \rho_{22} \end{pmatrix} \tag{5}$$

$$\rho_{ij} = 1 - \left(|S_{ij}|^2 + |S_{ij}|^2\right) \; and$$

$$\rho_{ij} = -\left(S_{ii}^* S_{ij} + S_{ji}^* S_{jj}\right) \quad for\ i, j = 1 or 2 \tag{6}$$

The measured variation of channel capacity loss (CCL) within operating frequency is under 0.7 bps/Hz, as shown in Fig. 23(b) which is acceptable for a practical MIMO system. The gain of the proposed UWB MIMO antenna is shown in Fig. 24, where the average gain of 4.72 dBi is obtained in the operating band.

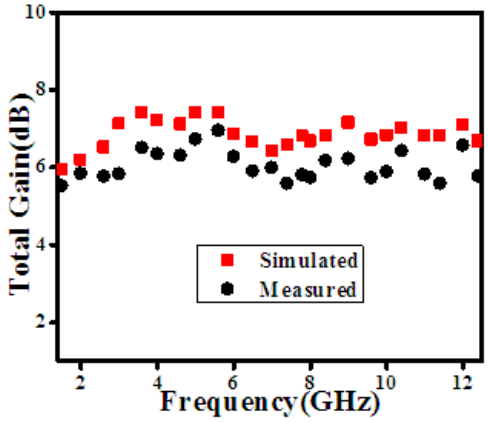

FIGURE 24. Simulated and measured results of the total gain of the proposed antenna.

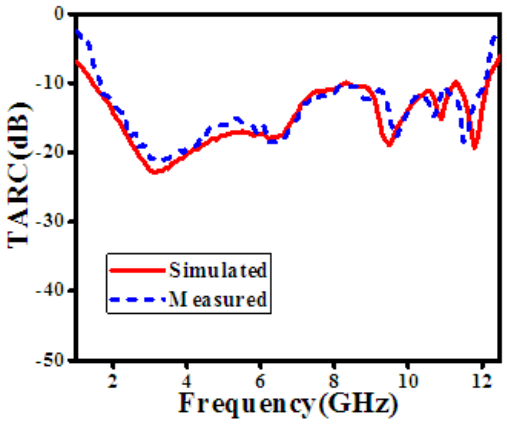

FIGURE 25. Simulated and measured results of TARC of the proposed antenna.

Fig. 25 shows the simulated and measured results of TARC of the proposed antenna. The simulated and measured results are slightly different due to presence of glue between the rectangular dielectric resonator antennas (RDRAs) and between the microstrip feed line network and the RDRAs. The radiation and total efficiency plot of the proposed antenna is depicted in Fig. 26. The radiation efficiency is approximately 89 % and total efficiency is approximately 88% throughout the operating frequency range.

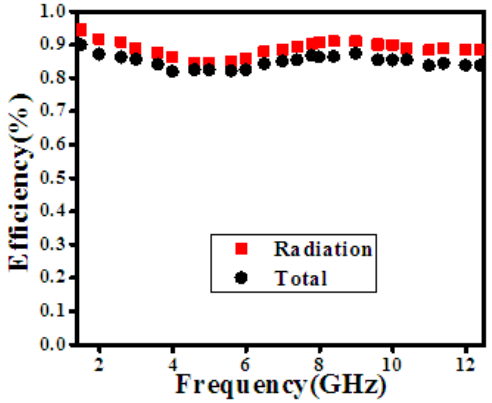

FIGURE 26. Simulation results of radiation efficiency of the proposed antenna.

V. CONCLUSION

In this letter, An Ultra wideband DRA is presented in MIMO configuration which has achieved 25 dB of isolation in the entire band (1.6-12.2 GHz) with 153.6% of impedance bandwidth. The ultra-wideband performance is dependent upon the shape and multipermittivity of RDRAs. Whereas, the isolation in the MIMO design has been achievd due to the combined effect of modified CPW feeding and extended metallic diagonal stub which minimizes the electromagnetic interation between the radiators.

REFERENCES

[1] E. G. Lim, Z. Wang, C. Lie and, K. L. Man, "Ultra wideband antennas—Past and present," *IAENG Int. J. Comput. Sci.*, vol. 37, pp. 304–314, 2010.
[2] M. Lapierre, Y. M. M. Antar, A. Ittipiboon, and A. Petosa, "Ultra wideband monopole/dielectric resonator antenna," *IEEE Microw. Wireless Compon. Lett.*, vol. 15, no. 1, pp. 7–9, Jan. 2005.
[3] K. S. Ryu and A. A. Kishk, "UWB dielectric resonator antenna having consistent omnidirectional pattern and low cross-polarization characteristics," *IEEE Trans. Antennas Propag.*, vol. 59, no. 4, pp. 1403–1408, Apr. 2011.
[4] M. Abedian, S. K. A. Rahim, S. Danesh, S. Hakimi, L. Y. Cheong, and M. H. Jamaluddin, "Novel design of compact UWB dielectric resonator antenna with dual-band-rejection characteristics for WiMAX/WLAN bands," *IEEE Antennas Wireless Propag. Lett.*, vol. 14, pp. 245–248, 2015.
[5] M. Shahzad Iqbal and K. P. Esselle, "Pulse-preserving characteristics and effective isotropically radiated power spectra of a new ultrawideband dielectric resonator antenna," *IET Microw., Antennas Propag.*, vol. 12, no. 7, pp. 1231–1238, Jun. 2018.
[6] M. Niroo-Jazi and T. A. Denidni, "Experimental investigations of a novel ultrawideband dielectric resonator antenna with rejection band using hybrid techniques," *IEEE Antennas Wireless Propag. Lett.*, vol. 11, pp. 492–495, 2012.
[7] R. Azim, M. T. Islam, and A. T. Mobashsher, "Design of a dual band-notch UWB slot antenna by means of simple parasitic slits," *IEEE Antennas Wireless Propag. Lett.*, vol. 12, pp. 1412–1415, 2013.
[8] S. F. Roslan, M. R. Kamarudin, M. Khalily, and M. H. Jamaluddin, "An MIMO rectangular dielectric resonator antenna for 4G applications," *IEEE Antennas Wireless Propag. Lett.*, vol. 13, pp. 321–324, 2014.
[9] A. J. Paulraj, D. A. Gore, R. U. Nabar, and H. Bolcskei, "An overview of MIMO Communications—A key to gigabit wireless," *Proc. IEEE*, vol. 92, no. 2, pp. 198–218, Feb. 2004.
[10] Y. Zhang, J.-Y. Deng, M.-J. Li, D. Sun, and L.-X. Guo, "A MIMO dielectric resonator antenna with improved isolation for 5G mm-wave applications," *IEEE Antennas Wireless Propag. Lett.*, vol. 18, no. 4, pp. 747–751, Apr. 2019.
[11] L. Liu, S. W. Cheung, and T. I. Yuk, "Compact MIMO antenna for portable devices in UWB applications," *IEEE Trans. Antennas Propag.*, vol. 61, no. 8, pp. 4257–4264, Aug. 2013.
[12] T. S. P. See and Z. N. Chen, "An ultrawideband diversity antenna," *IEEE Trans. Antennas Propag.*, vol. 57, no. 6, pp. 1597–1605, Jun. 2009.
[13] S. Wang and Z. Du, "Decoupled dual-antenna system using crossed neutralization lines for LTE/WWAN smartphone applications," *IEEE Antennas Wireless Propag. Lett.*, vol. 14, pp. 523–526, 2015.
[14] K. Wei, J. Y. Li, L. Wang, Z. J. Xing, and R. Xu, "Mutual coupling reduction by novel fractal defected ground structure band gap filter," *IEEE Trans. Antennas Propag.*, vol. 64, no. 10, pp. 4328–4335, 2016.
[15] M. S. Sharawi, "Current misuses and future prospects for printed multiple-input, multiple-output antenna systems [wireless corner]," *IEEE Antennas Propag. Mag.*, vol. 59, no. 2, pp. 162–170, Apr. 2017.
[16] G. Das, A. Sharma, R. K. Gangwar, and M. S. Sharawi, "Performance improvement of multiband MIMO dielectric resonator antenna system with a partially reflecting surface," *IEEE Antennas Wireless Propag. Lett.*, vol. 18, no. 10, pp. 2105–2109, Oct. 2019.
[17] N. Honma, H. Sato, K. Ogawa, and Y. Tsunekawa, "Accuracy of MIMO channel capacity equation based only on *S* -Parameters of MIMO antenna," *IEEE Antennas Wireless Propag. Lett.*, vol. 14, pp. 1250–1253, 2015.
[18] A. Petosa, *Dielectric Resonator Antenna Handbook*. Norwood, MA, USA: Artech House, 2007.
[19] R. K. Mongia and P. Bhartia, "Dielectric resonator antenna—A review and general design relations for resonant frequency and bandwidth," *Int. J. Microw. Millim.-Wave Comput. Aided Eng.*, vol. 4, no. 3, pp. 230–247, 1994.
[20] S. Keyrouz and D. Caratelli, "Dielectric resonator antennas: Basic concepts, design guidelines, and recent developments at millimeter-wave frequencies," *Int. J. Antennas Propag.*, vol. 2016, Sep. 2016, Art. no. 6075680.
[21] M. M. Sani, R. Chauwdhary, and R. K. Choudhary, "Electrically coupled dual semicylindrical dielectric resonator antenna with inverted arrangement for wideband applications," *Int. J. RF Microw. Comput. Aided Eng.*, vol. 29, no. 1, 2019, Art. no. 21928.
[22] C. Zebiri, H. A. Obeidat, R. A. Abd-Alhameed, D. Sayad, I. T. E. Elfergani, J. S. Kosha, W. F. A. Mshwat, C. H. See, M. Lashab, J. Rodriguez, and K. H. Sayidmarie, "Antenna for ultra-wideband applications with non-uniform defected ground plane and offset aperture-coupled cylindrical dielectric resonators," *IEEE Access*, vol. 7, pp. 166776–166787, 2019.
[23] Z. Song, H. Zheng, M. Wang, Y. Li, T. Song, E. Li, and Y. Li, "Equilateral triangular dielectric resonator and metal patch hybrid antenna for UWB application," *IEEE Access*, vol. 7, pp. 119060–119068, 2019.
[24] J. Iqbal, U. Illahi, M. I. Sulaiman, M. M. Alam, M. M. Suud, and M. N. M. Yasin, "Mutual coupling reduction using hybrid technique in wideband circularly polarized MIMO antenna for WiMAX applications," *IEEE Access*, vol. 7, pp. 40951–40958, 2019.
[25] A. Sharma and A. Biswas, "Wideband multiple-input–multiple-output dielectric resonator antenna," *IET Microw., Antennas Propag.*, vol. 11, no. 4, pp. 496–502, Mar. 2017.
[26] Y. Wang, N. Wang, T. A. Denidni, Q. Zeng, and G. Wei, "Integrated ultraw-ideband/narrowband rectangular dielectric resonator antenna for cognitive radio," *IEEE Antennas Wireless Propag. Lett.*, vol. 13, pp. 694–697, 2014.
[27] M. Abedian, S. K. A. Rahim, C. Fumeaux, S. Danesh, Y. C. Lo, and M. H. Jamaluddin, "Compact ultrawideband MIMO dielectric resonator antennas with WLAN band rejection," *IET Microw., Antennas Propag.*, vol. 11, no. 11, pp. 1524–1529, Sep. 2017.
[28] L. Y. Nie, X. Q. Lin, Z. Q. Yang, J. Zhang, and B. Wang, "Structure-shared planar UWB MIMO antenna with high isolation for mobile platform," *IEEE Trans. Antennas Propag.*, vol. 67, no. 4, pp. 2735–2738, Apr. 2019.
[29] Z. Li, C. Yin, and X. Zhu, "Compact UWB MIMO Vivaldi antenna with dual band-notched characteristics," *IEEE Access*, vol. 7, pp. 38696–38701, 2019.
[30] S. Zhang and G. F. Pedersen, "Mutual coupling reduction for UWB MIMO antennas with a wideband neutralization line," *IEEE Antennas Wireless Propag. Lett.*, vol. 15, pp. 166–169, 2016.
[31] J. Ren, W. Hu, Y. Yin, and R. Fan, "Compact printed MIMO antenna for UWB applications," *IEEE Antennas Wireless Propag. Lett.*, vol. 13, pp. 1517–1520, 2014.
[32] Z. Tang, X. Wu, J. Zhan, S. Hu, Z. Xi, and Y. Liu, "Compact UWB-MIMO antenna with high isolation and triple band-notched characteristics," *IEEE Access*, vol. 7, pp. 19856–19865, 2019.
[33] M. S. Sharawi, *Printed MIMO Antenna Engineering*. Norwood, MA, USA: Artech House, 2007.
[34] T. A. Denidni and Z. Weng, "Hybrid ultrawideband dielectric resonator antenna and band-notched designs," *IET Microw., Antennas Propag.*, vol. 5, no. 4, pp. 450–458, 2011.

MOHAMMAD MUZAMMIL SANI (Member, IEEE) was born in Jamshedpur, Jharkhand, India. He received the Bachelor of Engineering degree in electronics and communication engineering from Magadh University, Bodh Gaya, and the M.Tech. degree in electronic system and communication from the National Institute of Technology Rourkela. He is currently pursuing the Ph.D. degree with the Department of Electronics Engineering, IIT (Indian School of Mines), Dhanbad, India. He has worked as a Lecturer with the Department of Electronics and Communication Engineering, MACET, Patna, and the College of Computer Science and Information Systems, Jazan University, Jazan, Saudi Arabia. His current research interest includes dielectric resonator antennas and its application. He is a member of The Institution of Engineers, India.

RAKESH CHOWDHURY (Member, IEEE) was born in West Bengal, India, in September 1991. He received the B.Tech. degree in electronics and communication engineering from WBUT University, West Bengal, in 2013, and the M.Tech. degree from IIT (Indian School of Mines), Dhanbad, in 2015, where he is currently pursuing the Ph.D. degree. He has authored or coauthored more than 20 research articles in international journals/ conference proceedings. His current research interests include circularly polarized dielectric resonator antennas, high-gain antennas, and EBG structures. He received the Fellowship from the MHRD Government of India for his M.Tech. degree. He also received certificate of Honor for excelling in academics during graduation. He is a potential Reviewer of many journals, such as the IEEE Antennas and Wireless Propagation Letters, IEEE Access, the *International Journal of RF and Microwave Computer-Aided Engineering*, and AEU.

RAGHVENDRA KUMAR CHAUDHARY (Senior Member, IEEE) received the B.Tech. degree from UIET Kanpur, India, in 2007, the M.Tech. degree from IIT (BHU) Varanasi, India, in 2009, and the Ph.D. degree from IIT Kanpur, India, in 2014. He has researched in developing the metamaterial antenna and dielectric resonator antenna (DRA). One of his major areas of contribution is the development of the circularly polarized compact antenna. He is currently an Assistant Professor with the Department of Electronics Engineering, IIT (ISM), Dhanbad, India. He has published over 98 articles in top SCI journals. He has guided four Ph.D. students and currently 12 Ph.D. students are working under him. His current research interests include MIMO and cognitive radio, reconfigurable metamaterial/metasurface for antenna and absorber design, circularly polarized DRA, and frequency reconfigurable active array antenna with beam steering. He is a Senior Member of URSI. He was a recipient of the Young Engineers Award of the Institution of Engineers, India (IEI), from 2019 to 2020, and many Best Paper awards in different categories in national and international conferences, such as IEEE APACE, Malaysia; PIERS, Singapore; and ATMS, India. He has served as the Chair for the IEEE Student Branch of Uttar Pradesh Section, from 2012 to 2013. He has been serving as a Counselor for the IEEE Student Branch of IIT (ISM). He is a potential Reviewer of international journals such as the IEEE Transactions on Antennas and Propagation and the IEEE Antennas and Wireless Propagation Letters. He has also been featured interviewed by *IET Electronics Letters*, U.K. He has been serving as an Associate Editor for the *IET Microwave Antennas and Propagation*, U.K.; IEEE Access, USA; and *Microwave and Optical Technology Letters* (Wiley), USA.